Available online at www.sciencedirect.com
SCIENCE DIRECT
Journal of Catalysis 228 (2004) 362–373
JOURNAL OF CATALYSIS
www.elsevier.com/locate/jcat

Selective oxidation of propane to acrylic acid on K-doped MoVSbO catalysts: catalyst characterization and catalytic performance

T. Blasco [a], P. Botella [a], P. Concepción [a], J.M. López Nieto [a,*], A. Martinez-Arias [b], C. Prieto [c]

[a] *Instituto de Tecnología Química, UPV-CSIC, Avenida de los Naranjos s/n, 46022-Valencia, Spain*
[b] *Instituto de Catálisis y Petroleoquímica, Campus UAM Cantoblanco, 28049 Madrid, Spain*
[c] *Instituto de Ciencia de Materiales, CSIC, Cantoblanco, 28049 Madrid, Spain*

Received 22 June 2004; revised 23 August 2004; accepted 31 August 2004

Available online 28 October 2004

Abstract

K-doped Mo–V–Sb mixed oxides catalysts have been prepared by impregnation of a MoVSbO mixed oxide (previously prepared by hydrothermal synthesis) with an aqueous solution of potassium nitrate, characterized by XRD, SEM-EDX, EPR, XPS, XANES, and FTIR of adsorbed NH_3, and tested in the selective oxidation of propane and propylene in the 593–693 K temperature range. The undoped MoVSbO catalysts presented a selectivity to acrylic acid lower than 15%, while selectivities to acrylic acid of about 40% can be obtained on K-doped catalysts. No appreciable differences between undoped and K-doped catalysts are observed in the nature of crystalline phases present in each case, on the basis of X-ray diffraction analysis. However, important differences in both the oxidation state of surface Sb species (according to XPS evidence) and the number of acid sites (determined from FTIR of adsorbed NH_3) are observed between the undoped and the K-doped catalysts. The high selectivity to acrylic acid on the K-doped catalysts seems to be related to changes in the acid–base properties of the catalysts and most particularly to the elimination of (Brønsted) acid sites. In addition, the role of antimony species in activity and selectivity is also discussed and a reaction network for the partial oxidation reaction is proposed.

Keywords: Selective oxidation of propane to acrylic acid or acetic acid; K-doped Mo–V–Sb mixed metal oxide catalyst; Hydrothermal synthesis; Catalyst characterization (X-ray diffraction, XANES, EPR, XPS, FTIR of adsorbed ammonia)

1. Introduction

There is an increasing interest in the development of a process for direct oxidation of propane to acrylic acid as an alternative to the two-step conventional industrial process based on the propylene feedstock, which represents approximately 90% of the 1.84×10^6 tons/year of the total capacity of acrylic acid production plants [1,2]. Although a large number of catalytic systems have been studied, only few catalysts seem to be relatively active and selective [3,4]. This is the case of undoped and Me-doped V–P–O oxides [5–7], Ni–Mo–Te–P–O oxides [8,9], and metal and/or pyridine exchanged molybdovanadophosphoric acid [1–14].

MoVNbTe(Sb) catalysts have been recently proposed as active and selective in the oxidation of propane to acrylic acid [15–24], but the selectivities achieved on Sb-containing catalysts [19–23] are generally lower than those obtained on Te-containing catalysts [15–18]. Despite their practical interest, few fundamental studies on the nature and catalytic behavior of MoVSb-based catalysts have been published [20–23]. Although some factors seem to have an important influence on the selectivity to acrylic acid, such as the catalyst calcination conditions [20,21] or the incorporation of water in the feed [22], relatively low selectivities to acrylic acid have been reported.

Characterization results published on MoVSbO [23] and MoVSbNbO [20,21] catalysts suggest the presence of several crystalline phases depending on the chemical composition, the catalyst preparation procedure, and the calcina-

* Corresponding author. Fax: +34 96 3877809.
E-mail address: jmlopez@itq.upv.es (J.M. López Nieto).

0021-9517/$ – see front matter
doi:10.1016/j.jcat.2004.08.036

tion conditions. $Sb_4Mo_{10}O_{30}$ and $Sb_2Mo_{10}O_{31}$ in addition to $Mo_{5-x}(V/Nb)_xO_{14}$ were proposed to be present on samples prepared by a slurry method and heat-treated at 873 K in N_2 and activated in He or in O_2/He mixtures (20% of O_2), although some changes in the DRX were observed depending on the activation procedure [20,21]. $(Sb_2O)M_6O_{18}$ and $(SbO)_2M_{20}O_{56}$ (with M = Mo and V) were proposed, however, in MoVSbO catalysts prepared by hydrothermal synthesis and activated in air at 643 K for 20 min followed by a second heat treatment, in pure nitrogen, at 873 K for 2 h [26]. Nevertheless, the similarities of the XRD patterns of the oxides involved and the complexity of the systems render difficult an unambiguous interpretation of the diffraction data, and to get additional information, which may help to elucidate the crystallographic phases, present, by using other characterization techniques. In this sense, one of the differences among these crystalline phases is the Sb oxidation state, which is Sb^{3+} in $Sb_4Mo_{10}O_{30}$ and $Sb_2Mo_{10}O_{31}$ [20,25] and Sb^{3+}/Sb^{5+} in $(Sb_2O)M_6O_{18}$ and $(SbO)_2M_{20}O_{56}$ [26].

MoVSbO catalysts, prepared by hydrothermal synthesis, have also been studied in the partial oxidation of propane [23]. They present a selectivity to acrylic acid (ca. 6%) lower than that obtained on Te-based catalysts [16,23, 24], although their catalytic performance has partially been enhanced by grinding the catalyst precursor before the calcination step. However, selectivities to acrylic acid lower than 20% have been reported [23].

Recently, it has been shown that the selectivity to acrylic acid obtained during the selective oxidation of propane on MoVSbO catalysts can be improved by the incorporation of potassium on the catalyst surface [27]. This higher production of acrylic acid could be related to the modifications of the nature and number of acid sites on the catalyst surface after the incorporation of potassium. However, the role of each element and the nature of the crystalline phases are still unclear.

In this paper we will present the characterization and catalytic behavior of undoped and K-doped MoVSbO, in which the incorporation of potassium has a promoter effect on the catalytic performance for the selective oxidation of propane to acrylic acid. The characterization results show no changes in the bulk of the catalysts after the incorporation of potassium, suggesting that the higher selectivity to acrylic acid observed on K-doped catalysts could be mainly related to the modification of both the number and the nature of acid sites rather than changes in the oxidation state of the Sb cations on the catalyst surface.

2. Experimental

2.1. Catalyst preparation

A Mo–V–Sb mixed metal oxide catalyst was prepared by a hydrothermal method, using vanadyl sulfate, antimony sulfate, ammonium heptamolybdate, and water with a Mo/V/Sb atomic ratio of 1/0.18/0.15. The gel was autoclaved in Teflon-lined stainless-steel autoclave at 448 K for 48 h. The resulting precursor was filtered, washed, dried at 353 K for 16 h, and heat-treated at 873 K for 2 h in N_2 stream. It will be called the **MVS** sample.

K-doped Mo–V–Sb mixed metal oxide catalysts (with K/Mo atomic ratios from 0.002 to 0.02) have been prepared by impregnation of the **MVS** sample with aqueous solutions of potassium nitrate. The samples were then rotavapored at 323 K and 14 kPa. The resulting powders were dried overnight at 373 K and finally heat-treated at 773 K for 1 h in a N_2 stream. The samples will be named **MVSK**-n ($n = 1$ to 4); their main characteristics are shown in Table 1.

For comparative purpose, a portion of the MVS precursor was first calcined in air at 553 K (2 h) and then heat-treated at 873 K (2 h) in N_2. This sample will be referred to as **MVS-A-N**.

2.2. Catalyst characterization

X-ray diffraction patterns (XRD) were collected using a Philips X'Pert diffractometer equipped with a graphite monochromator, operating at 40 kV and 45 mA and employing nickel-filtered Cu$K\alpha$ radiation ($\lambda = 0.1542$ nm).

Scanning electron microscopy (SEM) and EDX microanalyses were performed on a JEOL JSM 6300 LINK ISIS instrument. The quantitative EDX analysis was performed using an Oxford LINK ISIS System with the SEMQUANT program, which introduces the ZAF correction.

Infrared spectra of the samples diluted in KBr (20 mg of the sample mixed with 100 mg of dry KBr and pressed into a disk) were obtained with a Nicolet 710 FTIR spectrometer.

Electron paramagnetic resonance spectra (EPR) were recorded with a Bruker ER-200D spectrometer working in the X-band and calibrated with a DPPH standard ($g = 2.0036$). Quantitative analysis was carried out by double integration of the EPR spectra and comparison with a copper sulfate ($CuSO_4 \cdot 5H_2O$) standard. Computer simulations were employed to determine experimental parameters or to quantify contributions of overlapping signals. Portions of ca. 40 mg of sample were introduced inside an EPR quartz probe cell and subjected (under conventional high vacuum conditions) to extensive room temperature outgassing prior to recording their spectra.

Photoelectron spectra (XPS) were recorded on a VG-Escalab-210 Spectrometer using Al$K\alpha$ radiation (Al$K\alpha$ = 1486 eV) operated at 12 kV and 20 mA. The spectrometer's hemispherical analyzer was set to 50 eV constant pass energy. The samples were previously outgassed at 373 K for 2 h in the preparation chamber of the spectrometer and subsequently transferred to the analysis chamber where the pressure during spectra acquisition was 5×10^{-10} Torr. The binding energy (BE) data were referenced to C1s (BE = 284.5 eV) from surface contamination. Atomic ratios of the elements were calculated from the relative peak areas

Table 1
Characteristics of undoped and K-doped Mo–V–Sb–O catalysts

Catalyst	S_{BET}[a]	K/Mo atomic ratio[b]	Mo–V–Sb–K atomic ratio[b]	Mo–V–Sb–K surface atomic ratio[c]	EDX analysis	
					Particle number[d]	Composition
MVS	9.5	0	$Mo_1V_{0.18}Sb_{0.15}$	$Mo_1V_{0.19-}Sb_{0.08}$	1	$MoV_{0.30}Sb_{0.34}$
					2–3–4	$MoV_{0.29–0.33}Sb_{0.18–0.20}$
					5–6	$MoV_{0.13–0.20}Sb_{0.18–0.20}$
					7	$MoV_{0.07}Sb_{0.05}$
MVSK-1	nd	0.002	$Mo_1V_{0.18}Sb_{0.15}K_{0.002}$	nd	nd	
MVSK-2	6.8	0.005	$Mo_1V_{0.18}Sb_{0.15}K_{0.005}$	nd	1–2	$MoV_{0.29–0.32}Sb_{0.18–0.20}K_{0.006–0.008}$
					3	$MoV_{0.24–0.26}Sb_{0.08–0.12}K_{0.006–0.008}$
					4	$MoV_{0.08}Sb_{0.05}K_0$
MVSK-3	nd	0.010	$Mo_1V_{0.18}Sb_{0.15}K_{0.01}$	$Mo_1V_{0.20}Sb_{0.10}K_{0.015}$	nd	
MVSK-4	6.6	0.020	$Mo_1V_{0.18}Sb_{0.15}K_{0.02}$	$Mo_1V_{0.21}Sb_{0.11}K_{0.016}$	1	$MoV_{0.22}Sb_{0.34}K_{0.004}$
					2–3–4–5–6	$MoV_{0.25–0.33}Sb_{0.12–0.20}K_{0.01–0.03}$
MVS-A-N	nd	0	$Mo_1V_{0.18}Sb_{0.15}$	$Mo_1V_{0.22}Sb_{0.17}$	nd	

[a] S_{BET} in $m^2\ g^{-1}$; nd = not determined.
[b] Chemical analysis was obtained by atomic absorption spectroscopy of heat-treated samples.
[c] Mo–V–Sb–K surface atomic ratio was determined by XPS.
[d] Particle number in Fig. 3.

of the respective core-level lines using the Wagner sensitivity factors [28]. The influence of the Kα3,4 satellite of the O1s line has been taken into account for the integration of the V2p3/2 core-level line. Thus, the satellite subtraction (intensity ratios I/I_0 and energies distances ΔE, between main line and satellite) has been adjusted by using a reference material without vanadium in order to obtain a smooth background baseline, as indicated in Ref. [29]. By optimising the above mentioned parameters, the values obtained for the satellite subtraction are Kα3: $I/I_0 = 0.06225$, $\Delta E = 9.8$ eV; and Kα4: $I/I_0 = 0.030$, $\Delta E = 11.8$ eV. Determination of the O1s peak area is calculated after subtraction of the Sb3d5/2 peak area (assuming a 3:2 peak ratio of the 3d5/2:3d3/2 doublets). Data analysis procedures involve smoothing, a Shirley background subtraction, and curve fitting using mixed Gaussian–Lorentzian functions by a least-squares method.

Sb L_I edge XANES spectra were acquired at room temperature at the line D42, XAS 13 beamline, at the LURE Synchrotron Radiation facility (Orsay, Paris) using a double crystal Si (311) monochromator, detuned until 50%. Detection was made in the transmission mode by using two ion chambers with air filled gas. Three scans were collected for every spectra in the range 4650–4680 eV, with varying energy steps in three regions: 0.5 eV/s between 4650 and 4680 eV, 0.2 eV/s in the 4680–4735 eV region, and 0.4 eV/s in the range 4735–4780 eV. Linear background absorption was subtracted to the entire spectra, which was then normalized at approximately 50 eV above the absorption edge. The spectrum of $FeSbO_4$ was recorded as a reference for the position of the Sb^{5+} cation, with the absorption maximum at 4707.5 eV.

Infrared spectra of adsorbed ammonia were obtained in a Bio-Rad Fis-4017 spectrophotometer. Wafers of 10 mg cm^{-2}, mounted in a Pyrex vacuum cell fitted with KRS-5 windows, were degassed at 473 K for 2 h and then cooled at room temperature. Ammonia was first admitted at room temperature, degassed for 1 h, and finally desorbed at 298–373 K.

2.3. Catalytic tests

The catalytic experiments were carried out in a fixed-bed quartz tubular reactor (i.d. 20 mm, length 400 mm), working at atmospheric pressure [24]. Catalyst samples (0.3–0.5 mm particle size) were introduced in the reactor and diluted with 2–4 g of silicon carbide (0.5–0.75 mm particle size) in order to keep a constant volume in the catalyst bed. The feed consisted of a mixture of $C_3H_8/O_2/H_2O$/He or $C_3H_6/O_2/H_2O$/He molar ratio of 4/8/30/58 or 4/9/30/57, respectively. Experiments were carried out in the 613–673 K temperature interval in order to achieve the highest selectivity to partial oxidation products. Reactants and reaction products were analyzed by on-line gas chromatography [16]. Blank runs showed that the homogeneous reaction could be neglected under the experimental conditions used in this work.

3. Results

3.1. Catalyst characterization

A slight decrease of the surface area is observed upon the incorporation of potassium in the MoVSbO catalyst (Table 1), indicating that neither the incorporation of potassium by impregnation nor a second heat-treatment in N_2 at 773 K for 1 h have a strong influence on the specific surface area of MoVSb-based catalysts.

The XRD pattern of the undoped MoVSbO catalyst is shown in Fig. 1a. The appearance of peaks at $2\theta = 22.3$, 25.8, 28.3, 36.3, 45.0, and 50.0° can be attributed to the presence of a Sb^{3+}-containing compound like $Sb_4Mo_{10}O_{30}$

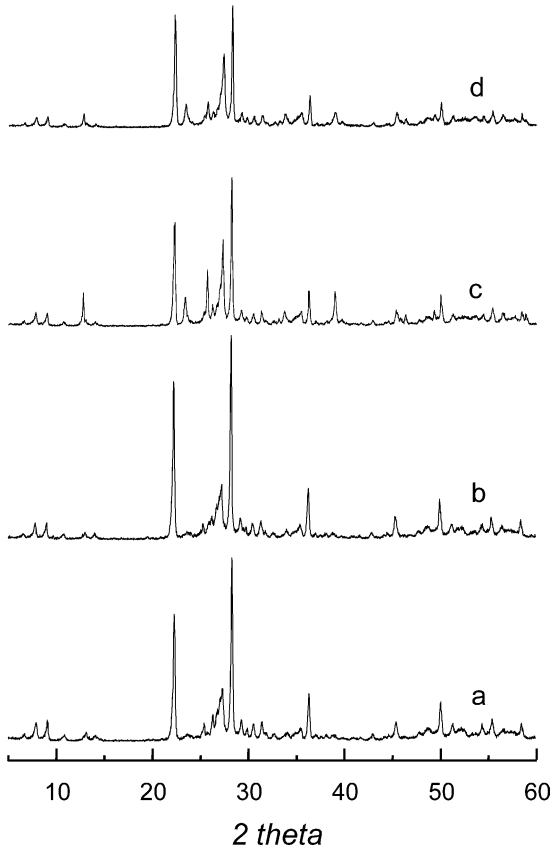

Fig. 1. XRD patterns of undoped and potassium-doped MoVSbO catalysts: (a) **MVS**; (b) **MVSK-4**; (c) **MVS-A-N**; (d) **MVS-A-N** after reaction test.

[JCPDS, 33-0104] [20,21], although the formation of $(Sb_2O)M_6O_{19}$ (with M = Mo and V), a Sb^{5+}/Sb^{3+}-containing crystalline phase [26] cannot be ruled out. Besides this, peaks at $2\theta = 6.6$, 7.8, 8.9, 22.3, 26.3, 26.7, 27.3, and 29.3° could be related to the presence of a Sb^{3+}-containing compound like $Sb_2Mo_{10}O_{31}$ [JCPDS: 33-105] [20,21], although the formation of $(SbO)_2M_{20}O_{56}$ (with M = Mo and V), a Sb^{5+}/Sb^{3+}-containing phase [26], $(V_{0.07}Mo_{0.93})_5O_{14}$ [JCPDS: 31-1437] should also be considered. No significant differences are appreciated in the XRD patterns when comparing undoped and K-doped MoVSbO samples (Fig. 1b), although changes in the proportion between $Sb_2Mo_{10}O_{31}/Sb_4Mo_{10}O_{30}$ or the presence of $(SbO)_2M_{20}O_{56}/(Sb_2O)M_6O_{18}$ cannot be detected by XRD. Furthermore, additional peaks at $2\theta = 12.9$, 25.4, 27.2, and 38.9° which can be due to the formation, as minor phases, of undoped or metal-doped MoO_3 [JCPDS: 5-508] are present in both the K-free and the K-doped samples. The intensity of these peaks is particularly high in the **MVS-A-N** sample (Fig. 1c). This suggests that, in this case, a partial oxidation of the catalyst is produced during the calcination in air at 553 K.

The morphology of the catalysts has been studied by scanning electron microscopy with X-ray energy dispersive analysis (EDX). The results obtained are collected in Table 1. The SEM image of the catalysts (not reported) shows

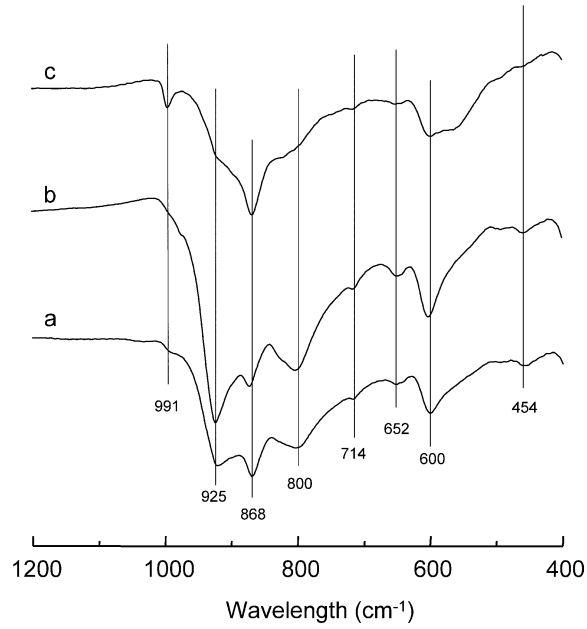

Fig. 2. IR spectra of undoped and K-doped catalysts: (a) **MVS**; (b) **MVSK-4**; (c) **MVS-A-N**.

the presence of agglomerates containing small slabs and rods of less than 5 μm in diameter. This morphology is similar to those previously observed in Te- [23,24] or Sb-based [23] catalysts prepared by hydrothermal synthesis. The global chemical composition obtained by EDX analysis is in fair agreement with those obtained by AAS (Table 1). Nevertheless, the SEM-EDX analysis evidences the presence of local inhomogeneities in the composition of the particles, with Sb-depleted zones, in some cases associated with lower V concentrations (Table 1). In every case, the composition of the crystals seems to be consistent with the crystalline phases observed by XRD.

Fig. 2 shows the IR spectra of undoped and K-doped catalysts. In agreement with the XRD results, the introduction of K in the Mo–V–Sb catalyst does not produce strong changes in the bulk of the catalyst, as no significant differences are found in the positions of the bands between samples with variable K content. The modifications observed in the overall or relative intensities of a determinate group of bands must rather be associated with K incorporation at surface positions. The bands at 868, 800, 714, and 652 cm^{-1} can be attributed to antisymmetric vibrations of Mo–O–Me (Me = Mo, Sb) bridging bonds [20,24,30]. The bands at ca. 925, 600, and 454 cm^{-1} are probably related to V=O groups and V–O–Me bonds (Me = Mo, V) [20,24,29] and/or to the presence of $Sb_2Mo_{10}O_{31}$ [20]. A shoulder at 990 cm^{-1} indicates the presence of Mo=O *cis*-dioxo groups of MoO_3 [30], which contribute to the band at 868 cm^{-1} too.

EPR spectra recorded at 77 K consist in all cases essentially in the overlapping of two signals. An example of spectrum deconvolution is shown in Fig. 3 for the **MVS** sample. All spectra basically consist in the overlapping of a major broad symmetric signal **A1** at $\langle g \rangle = 1.93$ with

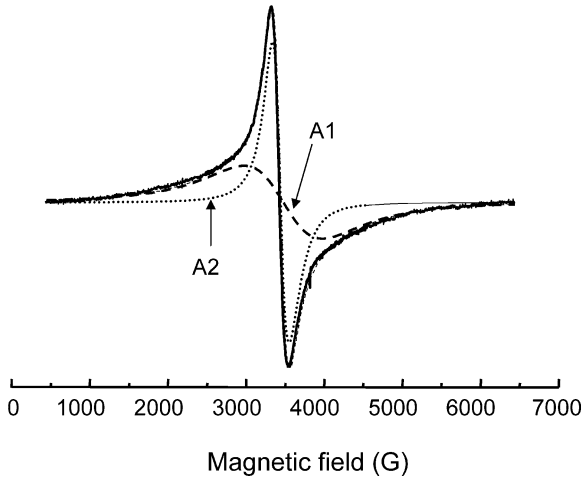

Fig. 3. Deconvolution of the EPR spectrum of sample **MVS** after its use in the catalytic test. The experimental spectrum is shown as a thicker gray line with the computer simulation being overlapped as a thinner black line and the individual signals as dotted black lines.

$\Delta H_{pp} \approx 1000$ G and a minor axial one at $g_{\perp} = 1.96$ and $g_{\parallel} = 1.90$, signal **A2**, which is narrower than the former (average width ≈ 225 G). It must be noted that signal **A1** could present certain anisotropy, difficult to be resolved as a consequence of its considerable width. Parameters of signals **A1** and **A2** are consistent with the presence of Mo^{5+} cations [16,31]; though their large linewidth does not discard the contribution of other possible paramagnetic cations (like V^{4+}), which could participate into magnetically coupled phases. This is particularly true for the major broader signal **A1**, for which a higher uncertainty in its estimated parameters could be inferred from computer simulations. In any case, the significant width of both signals, with the consequent absence of resolution of hyperfine features on them (it must be considered that ca. 25% of the molybdenum—^{95}Mo and ^{97}Mo isotopes—presents nuclear spin $I = 5/2$, while 99.75% of the vanadium presents $I = 7/2$), suggests that the paramagnetic centers are immersed into magnetically active environments (probably subjected to strong spin–spin interactions and of a considerable magnitude for centers giving rise to signal **A1**). In addition, some of the samples show a set of relatively narrow features overlapped on the spectrum of signals **A1** + **A2**, which corresponds to the presence of residual amounts of isolated V^{4+} species. Another signal represented by a feature appearing at $\langle g \rangle = 3.7$ is apparent for some of the samples, particularly **MVSK-2** and **MVSK-4**, although it can be also present in minor amounts for the other samples. This most likely corresponds to the forbidden transition ($\Delta m_s = \pm 2$) of Mo^{5+} ionic pairs in an excited triplet state [32], based on the fact that a certain intensity increase is observed upon recording the spectrum at 298 K. No systematic study of these aspects has been done since they do not appear of relevance in the context of the present work.

Concerning the quantitative aspects, the overall amount of paramagnetic species detected is 158.8, 167.1, and 178.1 μmol g^{-1}, for **MVS**, **MVSK-2**, and **MVSK-4** samples, respectively, which correspond to about 3% of the total amount of Mo. Concerning the relative contributions of signals **A1** and **A2**, the **A1**/**A2** intensity ratio displays, according to computer simulation results, values of 4.0, 5.0, and 5.3 for samples **MVS**, **MVSK-2**, and **MVSK-4**, respectively.

Binding energies at peak maximum and peak half widths (FWHM) of the V2p3/2, Mo3d5/2, Sb3d3/2, and K2p3/2 core-level lines in the XPS spectra of the **MVS**, **MVSK-2**, and **MVSK-4** samples, as well as the surface metal atomic ratio determined from XPS data, are given in Table 2. For comparative purposes, the XPS results of the MoVSbO sample calcined initially in air at 553 K and then in N_2 at 873 K (sample **MVS-A-N**) are also included. It can be noticed that the Mo/V/Sb surface atomic ratios of the catalysts remains almost the same after the incorporation of potassium and are in close agreement with the bulk composition (Table 1).

The FWHM values of the Mo3d peaks are similar in all samples and can be fitted with two components at BE = 232.7 and 231.7 eV for the Mo3d5/2 peak, which can be assigned to Mo^{6+} and Mo^{5+} species [24,33–35]. Noteworthy, a Mo^{5+}/Mo_{total} atomic ratio of about 0.35 (Mo^{6+}/Mo^{5+} molar ratio close to 2) is determined for samples calcined under N_2. This contrasts with detection of exclusively Mo^{6+} species for **MVS-A-N**, suggesting that a higher overall oxidation degree is achieved in this sample as a consequence of the intermediate calcination treatment under air performed in this sample, in agreement with XRD results.

The V2p3/2 core-level spectra of all samples can be decomposed into two components at BE = 516.3 and 517.4 eV, which can be assigned to V^{4+} and V^{5+}, respectively [24,35]. V^{4+} cations seem to be the main component in undoped and K-doped catalysts, presenting a V^{4+}/V_{total} atomic ratio of 0.84–0.87 (V^{4+}/V^{5+} molar ratio around 5.5) for **MVS** and **MVSK**-*n* samples (Table 3). No V^{3+} species have been detected in these catalysts. However, V^{3+} species (BE = 515.5 eV) are observed in sample **MVS-A-N**, which shows V^{4+}/V_{total} and V^{3+}/V_{total} atomic ratios of 0.61 and 0.29. So, a partial reduction of V^{4+} to V^{3+} is apparently produced for this sample.

While the addition of potassium to the MoVSb oxide does not appear to have a strong influence on the surface composition and the nature of V2p or Mo3d XPS spectra, a different behavior is inferred for Sb, according to the Sb3d XPS spectra (Fig. 4). The peak width of the Sb3d3/2 line is sensitively higher in the K-doped samples than in the samples without potassium (1.95 and 1.70 eV, respectively), which could be related to the presence of another species or to differential charging of the samples. Since no broadening has been observed in the peaks from other zones in the spectra of the K-doped samples, contributions from differential charging of the samples can be neglected. We must indicate that the identification of the Sb oxidation state is complicated because the Sb3d5/2 peaks overlap with O1s peaks and the BE separation of Sb^{3+} and Sb^{5+} is relatively small (approximately 0.6 eV). The deconvolution of the Sb3d3/2 line for

Table 2
XPS results of undoped and K-doped Mo–V–Sb–O catalysts

Sample	Binding energies (peak width)								Me^{n+}/Me_{total} atomic ratio		
	Mo3d5/2		V2p3/2			Sbd3/2		K2p3/2	Mo^{5+}/Mo_{total}	V^{4+}/V_{total} (V^{3+}/V_{total})[a]	Sb^{5+}/Sb_{total}
	Mo^{6+}	Mo^{5+}	V^{5+}	V^{4+}	V^{3+}	Sb^{5+}	Sb^{3+}				
MVS	232.7 (1.79)	231.8 (1.77)	517.4 (1.21)	516.3 (1.78)	–	–	539.5 (1.77)	–	0.35	0.87 (0)[a]	0
MVSK-3	232.7 (1.80)	231.7 (1.70)	517.3 (1.28)	516.3 (1.71)	–	540.2 (1.70)	539.4 (1.77)	292.9 (2.25)	0.26	0.84 (0)[a]	0.29
MVSK-4	232.8 (1.70)	231.9 (1.60)	517.4 (1.20)	516.3 (1.74)	–	540.4 (1.60)	539.5 (1.70)	293.1 (1.90)	0.35	0.84 (0)[a]	0.17
MVS-A-N	232.9 (1.80)	–	517.4 (1.20)	516.4 (1.60)	515.5 (1.60)	540.4 (1.69)	539.4 (1.70)	–	0	0.61 (0.29)[a]	0.81

[a] In parenthesis the V^{3+}/V_{total} atomic ratios calculated from the XPS experiments.

Table 3
Catalytic performance of undoped and K-doped MoVSbO mixed metal oxide catalysts in the selective oxidation of propane[a]

Catalyst	Conversion (%)[b]	Selectivity (%)[c]						
		CH_2:$CHCO_2H$	CH_3CO_2H	C_3H_6	CH_2:CHCHO	CH_3COCH_3	CO	CO_2
MVS	19.8	7.6	27.0	6.7	0.1	3.2	19.5	35.8
MVSK-1	14.3	19.8	16.2	11.5	–	4.6	15.3	32.7
MVSK-2	11.9	34.8	10.6	17.7	0.1	4.2	11.6	21.0
MVSK-3	9.5	34.5	8.4	22.2	–	3.5	11.1	20.3
MVSK-4	7.8	28.1	7.9	28.1	–	6.4	10.3	19.2
MVS-A-N	18.0	13.0	18.2	15.1	–	2.3	18.0	33.5

[a] Reaction conditions: Contact time, W/F, of 510 $g_{cat}\,h^{-1}\,mol^{-1}_{C_3H_8}$; reaction temperature: 613 K; $C_3H_8/O_2/H_2O$/He molar ratio of 4/8/30/58.

[b] Propane conversion (%).

[c] Acetaldehyde has also been observed with selectivities lower than 0.3%.

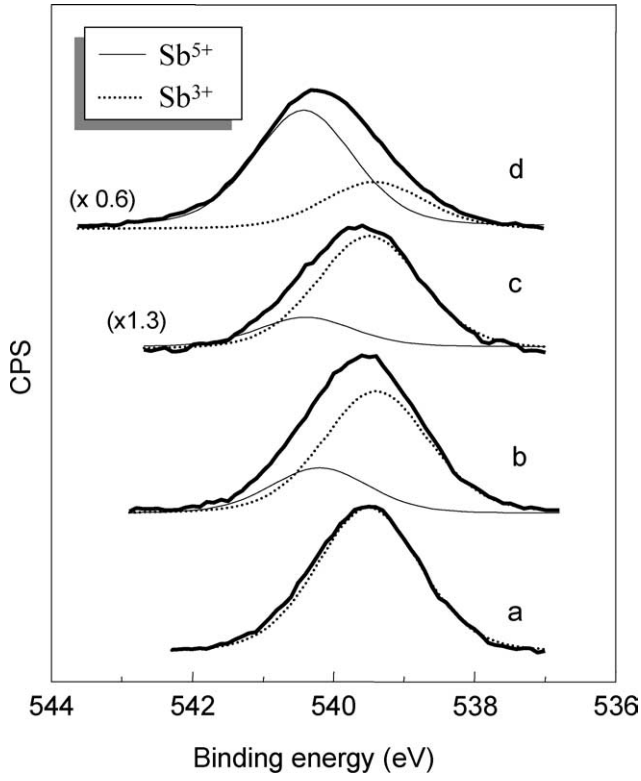

Fig. 4. XPS spectra of Sb3d3/2 in the undoped and K-doped MoVSbO catalysts: (a) **MVS**; (b) **MVSK-2**; (c) **MVSK-4**; (d) **MVS-A-N**.

the K-doped samples is shown in Fig. 4. The Sb3d3/2 peak of the K-containing samples can be fitted with two components at BE = 540.2 and 539.4 eV, assigned to Sb^{5+} and Sb^{3+}, respectively [26,36,37], while only one component at BE = 539.5 eV, of Sb^{3+}, is observed in the K-free sample.

These results suggest an oxidation of Sb^{3+} to Sb^{5+} on the catalyst surface (with Sb^{5+}/Sb_{total} atomic ratios of 0.17–0.29) after the incorporation of potassium. However, the formation of Sb^{5+} species is lower than that observed in the sample **MVS-A-N** (Sb^{5+}/Sb_{total} atomic ratios of 0.81). Such on-surface oxidation is not a consequence of the presence of oxygen during the calcination of these samples, but it could be related with the presence of nitrates (from the KNO_3 used to incorporate potassium) during the calcinations step. In fact, when the MoVSb precursor is calcined initially with O_2 and then with N_2 (sample **MVS-A-N**), the partial oxidation of Sb^{3+} to Sb^{5+} is accompanied by partial reduction of V^{5+} to V^{4+} and V^{3+}, although without apparent modification of the oxidation state of Mo (Mo^{6+}). At this point, it has to be said that in V–Sb-containing catalysts Sb^{5+} species are formed from Sb^{3+} at the expense of the partial reduction of V^{5+} to V^{4+} and V^{3+} [36,37], although, in the presence of Mo^{6+}, V^{3+} formed is rapidly oxidized to V^{4+} with the formation of Mo^{5+}.

Fig. 5 shows the normalized XANES region of the absorption spectra at the Sb L_I edge of samples **MVS**, **MVSK-3**, and **MVS-A-N** and those of $FeSbO_4$ and Sb_2O_3 used as

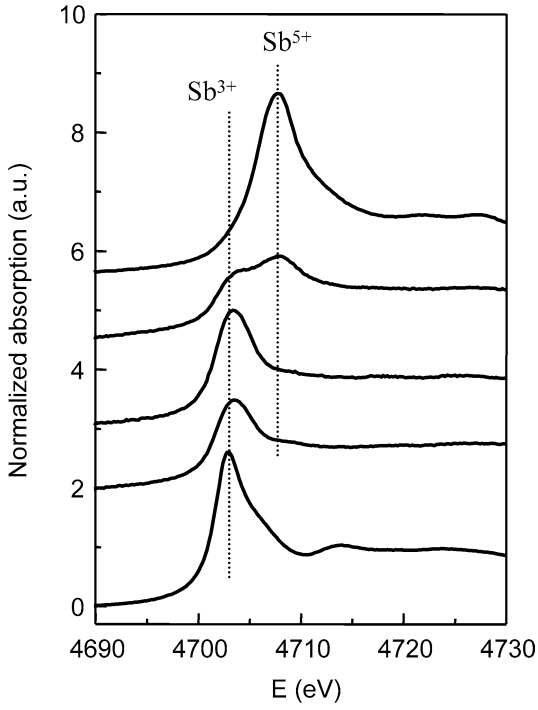

Fig. 5. Normalized XANES spectra at the Sb L_I edge of samples: (a) Sb_2O_3, (b) **MVS**, (c) **MVSK-3**, (d) **MVS-A-N**, and (e) $FeSbO_4$.

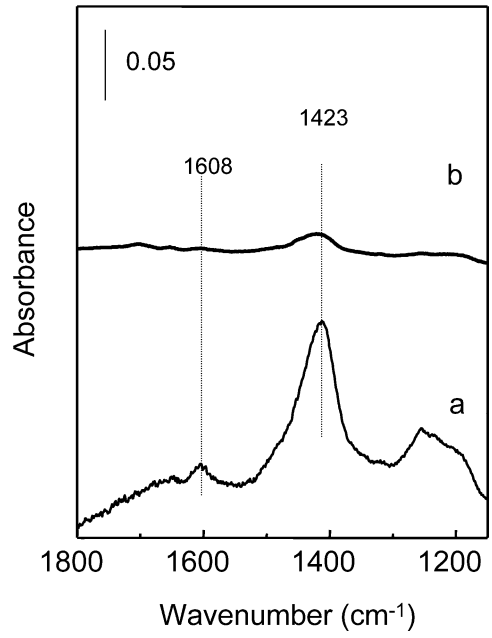

Fig. 6. FTIR spectra of NH_3 adsorbed on undoped and K-doped samples after evacuation at 373 K: (a) **MVS**; (b) **MVSK-3**.

references. The edge maximum corresponds to the electronic transition from the $2s_{1/2}$ to the empty 5p orbital, and the energy involved strongly depends on the occupancy of the 5s orbital, i.e., on the presence of Sb^{3+} or Sb^{5+}. The edge position is very sensitive to the oxidation state of antimony, appearing at 4703.0 eV for Sb^{3+} and at 4708.0 eV for Sb^{5+}, as can be observed for Sb_2O_3 and $FeSbO_4$, respectively, in Fig. 5. This renders XANES spectroscopy very valuable for determining the valence of antimony, information which is not easily available by any other technique.

The spectra of the K-free and K-containing **MVS** samples (see Fig. 5, spectra b and c) exhibit the edge maxima at 4703.4 eV, clearly indicating that antimony is present as Sb^{3+} in both oxides [26]. However, when the parent **MVS** oxide is calcined in air before the treatment in N_2, i.e., sample **MVS-A-N**, the maximum is shifted at 4708.0 eV characteristic of Sb^{5+}, while a shoulder at ca. 4703 eV of Sb^{3+} is also observed, evidencing the presence of antimony in both oxidation states (Fig. 5d). Fitting the spectrum using a combination of the two references for Sb^{3+} and Sb^{5+} the Sb^{3+}/Sb^{5+} ratio can be estimated to be approximately 1. Therefore, bulk oxidation of Sb^{3+} occurs upon the calcination in air of a MoVSbO sample (**MVS-A-N**) but not upon incorporation of potassium.

Reported in Fig. 6 are the infrared spectra of ammonia adsorbed on undoped (Fig. 6a) and K-doped (Fig. 6b) MoVSbO catalysts after evacuation at 373 K. The adsorption band at 1608 cm^{-1} can be attributed to the asymmetric bending vibration of ammonia adsorbed on Lewis acid sites, while the band at 1423 cm^{-1} corresponds to an asymmetric deformation vibration (δ_{as}) of the ammonium ions (NH_4^+) on Brønsted acid sites [38]. The broadening of the latter band must be related to a certain heterogeneity in the Brønsted acid sites, or to a splitting of the δ_{as} vibration as a consequence of changes in the adsorption symmetry of the NH_4^+ molecule at the catalyst surface.

The incorporation of potassium apparently decreases the intensity of both bands, thus confirming the diminution of the number of acid sites of the catalyst as already observed upon incorporation of alkali metals on V- or Mo-based catalysts [39–43].

Conversely, no significant structural changes have been detected by XRD in the **MVS** and K-doped catalysts after the catalytic test, and only the **MVA-A-N** sample shows a slight decrease in the intensity of the peaks corresponding to MoO_3 (Fig. 1d). The XPS study of the undoped and K-doped MoVSbO used samples shows neither changes in the catalyst composition nor important variations in the oxidation state of each element on the catalyst surface. In addition, Sb^{3+} was also mainly observed by EXAFS in the used catalysts. Therefore, we can assume that, under the reaction conditions used in this work, our catalysts are reasonably stable during the reaction tests.

3.2. Catalytic results for the selective oxidation of propane

Fig. 7 reports the variation of the propane conversion and the selectivities to the main reaction products obtained during the oxidation of propane in the 613–673 K temperature range, while Table 3 summarizes the catalytic results obtained during the oxidation of propane at 653 K on undoped and K-doped catalysts. Partial oxidation products (propylene, acrylic acid, acrolein, acetone, and acetic acid) and

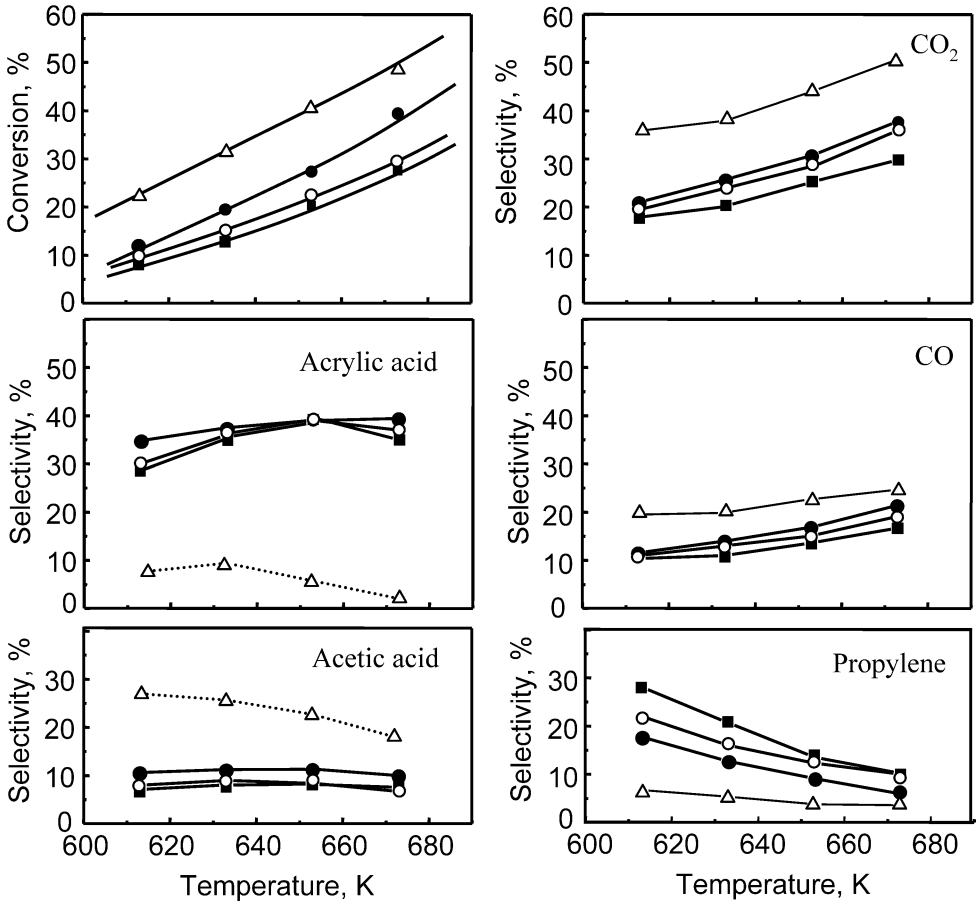

Fig. 7. Variation of the propane conversion and the selectivities to the main reaction products with the reaction temperature obtained during the oxidation of propane at 653 K over the undoped and K-doped catalysts: **MVS** (△); **MVSK-2** (●); **MVSK-3** (○); **MVSK-4** (■). Contact time, W/F, of 510 $g_{cat}\,h^{-1}\,mol_{C3}^{-1}$.

carbon oxides have been observed in all cases, although their corresponding selectivities strongly depend on the catalyst composition.

The undoped **MVS** sample presents a very low selectivity to acrylic acid but an important selectivity to acetic acid. Comparing the samples **MVS** and **MVS-A-N**, it can be concluded that no apparent modification in the catalytic performance occurs when the sample is previously calcined in air at 553 K before the heat treatment at 873 K in N_2 (Table 3).

The catalytic behavior of MoVSbO catalysts is completely modified when potassium is added to the catalyst (Fig. 7 and Table 3). The incorporation of small amounts of potassium notably increases the selectivity to acrylic acid and propylene, decreasing the selectivity of both acetic acid and carbon oxides. However, the propane conversion decreases with increasing the K content in the catalyst. In this way the sample with a K/Mo ratio of 0.02 presents less than half of propane conversion than the undoped samples.

A relative increase in the selectivity to organic acids (acrylic and acetic acids) without apparent changes in the propane conversion has been obtained when a MoVSbO catalyst was treated with a K-free aqueous solution following a procedure similar to that used for the preparation of the K-containing samples [27] or by grinding a $Mo_6V_2SbO_x$ catalyst [23]. However, the increase in the selectivity to acrylic acid in the last two cases was very modest compared to the changes obtained for the K-doped catalysts. So, the changes observed in the K-doped catalysts cannot be explained by mechanical modifications of the crystalline phases, but by the effect of K-induced modification of the catalyst surface.

The results of Fig. 7 indicate that the selectivity to propylene decreases and the selectivity to acrylic acid increases when the reaction temperature increases. However, the effect of the reaction temperature on the selectivity to acrylic acid is a consequence of the variation of the propane conversion. In this way, the highest selectivity to acrylic acid was observed at propane conversions between 20 and 30%.

The yields of partial oxidation products, i.e., acrylic acid, propylene, and acetic acid, obtained at 653 K over the studied catalysts are reported in Fig. 8. An opposite trend in the yields of acetic and acrylic acids is observed when the amount of potassium incorporated to the catalysts is increased, whereas the yield of propylene remains almost unchanged. Moreover, no changes in the sum of the yield of partial oxidation products (acrylic acid, acetic acid, and propylene) are apparently observed when the amount of potassium on the catalysts is changed. Therefore, the

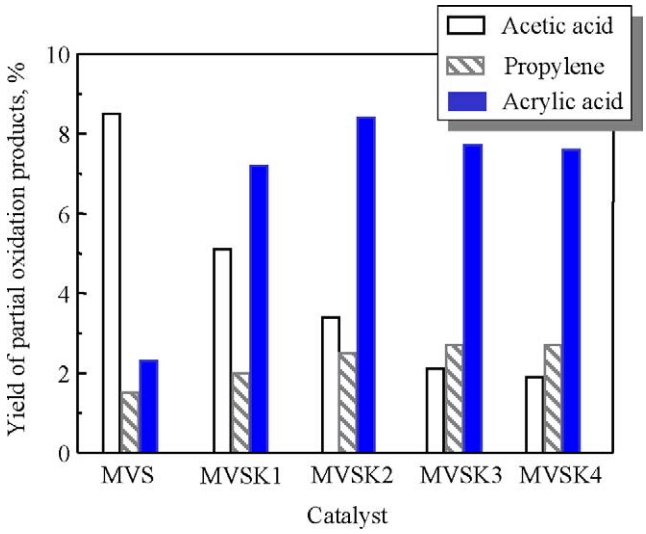

Fig. 8. Yield of acetic acid, propylene, and acrylic acid obtained during the oxidation of propane at 653 K over undoped and K-doped samples. Contact time, W/F, of 510 $g_{cat}\,h^{-1}\,mol^{-1}_{C3}$.

lower conversion observed in the K-doped catalysts must be mainly related to a decrease in the formation of carbon oxides. So, the incorporation of potassium favors an enhancement of both the selectivity and the yield of acrylic acid by decreasing the formation of both acetic acid and carbon oxides. It must be noted that the yields to acrylic acid obtained over the K-doped samples are higher than those previously reported in the literature for MoVSbO [23] or Nb-containing MoVSbO catalysts [20–22], although lower than those reported in the patent literature [19,44].

In order to gain a better understanding of the different pathways in the mechanism for propane oxidation, we have carried out some experiments of propylene oxidation, since propylene can be considered as intermediate in propane oxidation. Table 4 shows the catalytic results obtained during the propylene oxidation on undoped and K-doped catalysts. Acrylic acid, acetic acid, acetone, and carbon oxides are mainly observed, while acrolein and acetaldehyde were detected with very low selectivities. Acetone was the most important partial oxidation reaction product at low temperatures and low propylene conversions, while acrylic acid (mainly obtained on K-doped catalysts) and/or acetic acid (mainly obtained on undoped **MVS** samples) were obtained at high reaction temperatures and high propane conversions. This trend is similar to that observed during the propane oxidation.

4. Discussion

4.1. On the catalyst characterization

The characterization results presented here suggest that the incorporation of K modifies only the characteristics of the surface of the MoVSbO catalyst, although whether changes in the nature of the crystalline phases are induced is still unclear. The XRD patterns of K-free and K-doped catalysts suggest the presence of similar crystalline phases. According to this, SEM/EDX results indicate the presence of essentially two compositionally different zones in the catalysts. Vanadium appears homogeneously distributed in the crystallites, which suggests that it is incorporated to the structure of Mo–Sb–O mixed oxide, as already proposed for Mo–V–Te–Nb–O [24] and Mo–V–Sb–O mixed oxides [23]. However, the XRD by itself cannot be used in the determination of the crystalline phases in these catalysts. In fact, recent results published on MoVSbO [23] and MoVSbNbO [20,21] catalysts suggest the presence of several SbMoVO crystalline phases depending on the calcination conditions: $Sb_4Mo_{10}O_{30}$ and $Sb_2Mo_{10}O_{31}$ in samples heat-treated at 873 K in N_2 and activated in He [20,21] and $(Sb_2O)M_6O_{18}$ and $(SbO)_2M_{20}O_{56}$ (with M = Mo and V) in samples activated in air at 643 K for 20 min followed by a second heat treatment, in pure nitrogen, at 873 K for 2 h [26]. Moreover, the XRD pattern of $Sb_4Mo_{10}O_{30}$ is similar to that shown by $(Sb_2O)M_6O_{18}$, while the XRD pattern of $Sb_2Mo_{10}O_{31}$ is similar to that of $(SbO)_2M_{20}O_{56}$, making difficult an un-

Table 4
Catalytic performance of undoped and K-doped MoVSbO mixed metal oxide catalysts in the selective oxidation of propylene[a]

Catalyst	Temperature (K)	Conversion (%)[b]	Selectivity (%)[c]					
			CH_2:$CHCO_2H$	CH_3CO_2H	CH_2:CHCHO	CH_3COCH_3	CO	CO_2
MVS	593	42.9	27.0	8.4	0.2	35.3	14.5	14.4
	613	56.3	32.0	12.4	0.1	14.7	21.5	19.2
	638	68.4	21.0	13.0	0.1	6.0	36.0	33.4
MVSK-2	614	29.1	36.6	6.3	0.3	31.6	13.2	12.0
	636	39.1	46.4	7.7	0.2	14.3	17.0	14.3
	653	50.6	46.0	7.5	0.1	5.8	22.2	18.4
MVSK-4	613	19.0	36.0	3.0	0.5	42.0	10.2	8.3
	634	27.8	51.1	4.8	0.4	19.7	13.7	10.3
	654	34.9	59.6	4.1	0.3	7.7	16.1	12.1

[a] Reaction conditions: $C_3H_6/O_2/H_2O$/He molar ratio of 4/9/30/57 and contact time, W/F, of 100 $g_{cat}\,h^{-1}\,mol^{-1}_{C_3H_6}$.

[b] Propylene conversion (%).

[c] Acetaldehyde was also observed with a selectivity lower than 0.3%.

ambiguous attribution of the diffraction peaks. The most important differences among these crystalline phases appear to be related to the oxidation states of Sb: only Sb^{3+} is present in $Sb_4Mo_{10}O_{30}$ and $Sb_2Mo_{10}O_{31}$ [20,25], while Sb^{3+} and Sb^{5+} are observed in $(Sb_2O)M_6O_{18}$ (with a Sb^{3+}/Sb^{5+} ratio of 63/37) and $(SbO)_2M_{20}O_{56}$ (with a Sb^{3+}/Sb^{5+} ratio of 11/89) [26]. So, a possible discrimination between these structures could be established on the basis of the presence of Sb ions with different oxidation states.

Therefore, the presence of both Sb^{3+} and Sb^{5+} in **MVS-A-N**, determined by XANES, suggests the possible presence of $(Sb_2O)M_6O_{18}$ and $(SbO)_2M_{20}O_{56}$ (with M = Mo and V), rather than $Sb_4Mo_{10}O_{31}$ and $Sb_2Mo_{10}O_{31}$ [26], in catalysts first calcined in oxygen and then heat-treated in N_2. Sb^{5+} species have not been observed by XANES in both undoped and K-doped catalysts heat-treated in N_2, i.e., **MVS** and **MVSK-n** series, suggesting the presence of $Sb_4M_{10}O_{31}$ and $Sb_2M_{10}O_{31}$ (with M = Mo and V). Only a partial oxidation of surface Sb^{3+} to Sb^{5+} species, which are not observed in the undoped sample, and a decrease in the number of acid sites, especially of Brønsted type, are observed upon the addition of potassium on the surface of the MoVSbO mixed oxide.

The EPR experiments evidence the presence of two different magnetic environments for the paramagnetic cations (Mo^{5+} and possibly also V^{4+}), corresponding to signals **A1** and **A2**. It is tempting to establish a correlation between the two signals and the presence of two distinct phases (as suggested also by the EDX results of Table 1) into which the corresponding paramagnetic species would be immersed. The larger width of signal **A1** suggests shorter average distances between the spins, and then a higher concentration of Mo^{5+} (and V^{4+}) species would be expected in this magnetic domain. It must be noted that the amount of paramagnetic species detected in these spectra is relatively low when compared to the total amount of Mo and V (around 3%, considering the sample compositions determined by AAS, Table 1). The considerable higher concentration of paramagnetic species obtained by XPS (Table 2) and the low surface area of these oxides (Table 1) would suggest that they are exclusively located at surface or near surface. However, this is not consistent with the presence of mixed valence (Mo^{6+}/Mo^{5+} or V^{5+}/V^{4+}) phases observed by XRD. In fact, the EPR spectrum of sample **MVS** recorded under air (at atmospheric pressure) shows almost no modification in the signals lineshape or amplitude, suggesting a bulk nature for most of the detected paramagnetic centers. Therefore, it appears that a significant amount of the paramagnetic species must escape detection due to antiferromagnetic couplings [45].

Moreover, the relatively low amount of Sb^{5+} species detected by XPS on the surface of K-doped catalysts and the fact that Sb^{5+} species are not detected by XANES, along with consideration that structural or chemical transformations induced by K ions must mainly affect the catalyst surface, suggest that oxidized Sb^{5+} is only located on the catalyst surface. A different conclusion can be proposed in the sample initially calcined in air and then heat-treated in N_2 (sample **MVS-A-N**). The XPS spectra of this sample suggest a high Sb^{5+}/Sb^{3+} ratio on the surface, besides several oxidation states for V, i.e., V^{5+}, V^{4+}, and V^{3+}, with a higher overall reduction state. These results suggest that a different solid-state reaction occurs upon calcination of the sample under oxygen, which favors a redox reaction between V and Sb, as suggested in other V–Sb–O-based catalysts [35,36].

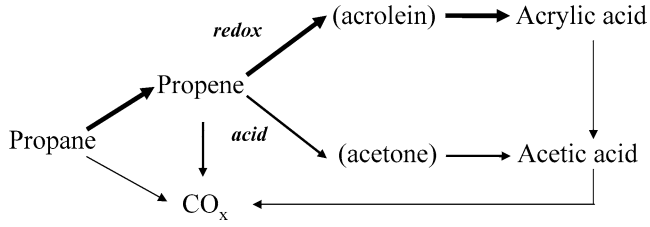

Scheme 1. Reaction network for the oxidation of propane on MoVSb-based catalysts.

4.2. Selective oxidation of propane on undoped and K-doped MoVSbO catalysts

According to our results, a reaction network of propane oxidation similar to that previously reported for MoVTe- [16,24,46,47] or MoVSb-based [20–23] catalysts can be proposed (Scheme 1), with a higher selectivity to acetone and acetic acid over the latter. Propylene is initially formed from propane on both undoped and K-doped catalysts. According to the results of Table 4, propylene can consecutively react on the catalyst surface giving three parallel reactions: (i) partial oxidation to acrolein/acrylic acid; (ii) hydration and oxidative scission to acetone/acetic acid; (iii) direct oxidation to carbon oxides. It is clear that the modification of the catalyst surface by the K incorporation strongly changes the reaction rates of the parallel reactions. In this way, a higher formation of acrylic acid and a lower formation of acetic acid and carbon oxides have been observed in the K-doped catalysts (Fig. 7).

It is generally accepted that both the selective oxidation and the oxidative dehydrogenation of propane are initiated via H abstraction from propane by a concerted mechanism over acid–base pairs [3,4,16–18,21–24]. The Lewis acid site (V^{5+} cation) and basic oxygen (O^{2-}) interacts with the α- and β-hydrogen of propane, respectively, to form propylene [24,48]. The incorporation of K ions on the surface of V- [39–41] or Mo-based [41–43] catalysts has been reported to modify the acid character and the nature of surface metal species, favoring the achievement of higher selectivities to propylene from propane. Accordingly, the incorporation of potassium to MoVSbO catalysts is expected to increase the selectivity to propylene during the oxidative dehydrogenation [39–43], but it is apparently surprising the fact that the selectivity to acrylic acid is also increased.

It is known that acid sites favor the formation of acetic acid, and that V_2O_5–MoO_3 catalyst favors the oxidative scis-

sion of propylene in the presence of water vapor to form acetone/acetic acid [49]. Meanwhile, alkaline cations promote the allylic oxidation of propylene or butylenes over Mo-containing catalysts [50,51]. According to these results, the incorporation of potassium to the MoVSbO catalyst surface decreases the number of acid sites, and then the formation of both acetic acid and carbon oxides. A similar effect is observed upon the addition of H_2O in the feed, which enhances the selectivity to acrylic acid during the oxidation of propane on MoVSbNbO [22] or VPO [6]. So, it appears that the elimination of the strongest acid sites favors the partial oxidation rather than the hydration (and the oxidative scission) reaction.

Beside the decrease in the surface acidity, the incorporation of K on the surface of the MoVSbO catalyst provokes the partial oxidation of surface Sb^{3+} to Sb^{5+}, which could favor the formation of acrylic acid by an allylic mechanism [18]. However, the catalytic results over **MVS** (Sb^{3+}) and **MVS-A-N** (Sb^{3+}/Sb^{5+}) suggest no apparent influence of the oxidation state of Sb on catalytic behavior, and then that the increase in the selectivity to acrylic acid on K-doped MoVSbO catalysts must be mainly due to changes in the catalyst acidity.

At the moment, it is not possible to establish the position of K^+ cations at the catalyst surface. Potassium could be located over oxygen atoms of Mo, V, or Sb, replacing surface protons and giving rise to Me–O–K surface bonds, or into the empty channels of the crystalline phases. Though the K^+ cations seems to favor, directly or indirectly, the appearance of Sb^{5+} species on the catalyst surface, the mechanism is still unclear. A higher effort will be made in order to clarify the nature of active sites in each reaction step (oxidative dehydrogenation, O insertion or oxidative scission) as well as the sites in which potassium cations are incorporated.

5. Conclusions

In conclusion, the incorporation of potassium on the surface of MVSbO catalysts enhances the formation and the selectivity to acrylic acid and decreases the formation of acetic acid and carbon oxides during the oxidation of propane. The presence of potassium diminishes the acidity of the catalyst surface, avoiding undesiderable reactions and favoring the selective formation of acrylic acid.

No important modification in the characteristics of the catalysts has been observed after the incorporation of potassium. In fact, the main characterization results (XRD, SEM, EDX, FTIR, EPR, and XANES) suggest clearly that $Sb_4M_{10}O_{30}$ and $Sb_2M_{10}O_{31}$ (with Sb^{3+} and M = Mo and V) are mainly present in undoped and K-doped catalysts heat-treated in N_2, whereas $(Sb_2O)M_6O_{18}$ and $(SbO)_2M_{20}O_{56}$ (with Sb^{3+}/Sb^{5+} and M = Mo and V) can be proposed as major phases in the sample first calcined in air and then heat-treated in N_2. Moreover, a partial oxidation of Sb^{3+} to Sb^{5+} (Sb^{5+}/Sb_{total} of 0.2–0.3) is observed on the surface of the K-doped catalysts, probably as a consequence of the presence of nitrates during the calcination of doped samples.

A further "in-situ" study of these catalysts will help to determine the exact nature of crystalline phases and the possible incorporation of V species in the structure of Mo–Sb–O mixed oxides.

Acknowledgments

This work was carried out under the financial support of the Spanish CICYT (Project PPQ2003/03946). Thanks are due to Dr. A. Mifsud for her discussion in SEM/EDX results and Prof. J. Soria for the use of the EPR spectrometer. The authors thank LURE for technical assistance and by the inclusion in the European Training and Mobility Program, special thanks are given to Dr. A. Traverse.

References

[1] R.E. Kirk, F. Orthmer, J.I. Kroschwitz, M. Howe-Grant, Kirk-Othmer's Enciclopedia of Chemical Technology, Wiley, New York, 1991.
[2] N. Nojiri, Y. Sakai, Y. Watanabe, Catal. Rev. Sci. Eng. 37 (1995) 145.
[3] T. Ushikubo, Catal. Today 78 (2003) 43.
[4] M.M. Lin, Appl. Catal. A 207 (2001) 1.
[5] M. Ai, Catal. Today 42 (1988) 297.
[6] G. Landi, L. Lisi, J.C. Volta, Chem. Commun. (2003) 492.
[7] Y.-F. Han, H.-M. Cheng, H. Wang, J.F. Deng, Chem. Commun. (1999) 521.
[8] A.C. Kaddouri, C. Mazzocchia, E. Tempesti, Appl. Catal. A 180 (1999) 271.
[9] N. Fujikawa, K. Wakui, K. Tomita, W. Onoe, W. Ueda, Catal. Today 71 (2001) 83.
[10] N. Mizuno, M. Tateishi, M. Iwamoto, Appl. Catal. A 128 (1995) L165.
[11] H.-S. Jiang, X. Mao, S.-J. Xie, B.-K. Zhong, J. Mol. Catal. A 185 (2002) 143.
[12] W. Li, K. Oshihara, W. Ueda, Appl. Catal. A 182 (1999) 357.
[13] J.H. Holles, C.J. Dillon, J.A. Labinger, M.E. Davis, J. Catal. 218 (2003) 42.
[14] M.E. Davis, C.J. Dillon, J.H. Hollesand, J.A. Labinger, Angew. Chem. Int. Ed. 41 (2002) 858.
[15] T. Ushikubo, N. Hiroya, K. Yukio, W. Shin, US patent 5,380,993 (1995).
[16] P. Botella, J.M. López Nieto, B. Solsona, A. Martinez-Arias, Catal. Lett. 74 (2001) 149.
[17] H. Tsuji, Y. Koyasu, J. Am. Chem. Soc. 124 (2002) 5608.
[18] R.K. Grasselli, J.D. Burrington, D.J. Buttrey, P. DeSanto, C.G. Lugmair, A.F. Volpe, T. Weingand, Top. Catal. 23 (2003) 5.
[19] H. Hinago, K. Hiroyuki, DE patent 10,145,958 A1 (2001).
[20] J.C. Vedrine, E.M. Novakova, E.G. Derouane, Catal. Today 81 (2003) 27.
[21] E.M. Novakova, J.C. Vedrine, E.G. Derouane, J. Catal. 211 (2002) 235.
[22] E.M. Novakova, E.G. Derouane, J.C. Vedrine, Catal. Lett. 83 (2002) 177.
[23] W. Ueda, K. Oshihara, Appl. Catal. A 200 (2000) 135.
[24] P. Botella, J.M. López Nieto, B. Solsona, A. Mifsud, F. Márquez, J. Catal. 209 (2002) 445.
[25] M. Parmentier, C. Gleitzer, R.J.D. Tilley, J. Solid State Chem. 31 (1980) 305.
[26] J.M.M. Millet, M. Baca, A. Pigamo, D. Vitry, W. Ueda, J.L. Dubois, Appl. Catal. A 244 (2003) 359.

[27] P. Botella, P. Concepción, J.M. López Nieto, B. Solsona, Catal. Lett. 89 (2003) 249.
[28] C.D. Wagner, L.E. Davis, M.V. Zeller, T.A. Taylor, R.H. Raymond, L.H. Gale, Surf. Interface Anal. 3 (1981) 211.
[29] M. Wark, M. Koch, A. Bückner, W. Grünert, J. Chem. Soc., Faraday Trans. 94 (1998) 2033.
[30] J.C.J. Bart, F. Cariati, A. Sgamelloti, Inorg. Chim. Acta 36 (1979) 105.
[31] K. Dyrek, M. Che, Chem. Rev. 97 (1997) 305.
[32] E. Abi-Aad, A. Bennani, J.-P. Bonnelle, A. Aboukais, J. Chem. Soc., Faraday Trans. 91 (1995) 99.
[33] K. Asakura, K. Nakatani, T. Kubota, Y. Iwasawa, J. Catal. 194 (2000) 309.
[34] J.M.M. Millet, H. Roussel, A. Pigamo, J.L. Dubois, J.C. Jumas, Appl. Catal. A 232 (2002) 77.
[35] V. Bondarenka, S. Grebinskij, S. Kaciulis, G. Mattogno, S. Mickevicius, J. Electron Spectrosc. Relat. Phenom. 107 (2000) 253.
[36] J. Nilson, A.R. Landa-Cánovas, S. Hansen, A. Andersson, J. Catal. 186 (1999) 442.
[37] A. Andersson, S.L.T. Andersson, G. Centi, R.K. Grasselli, M. Sanati, F. Trifiró, Appl. Catal. A 113 (1994) 43.
[38] H. Knözinger, in: G. Ertl, H. Knözinger, J. Weitkamp (Eds.), Handbook of Heterogeneous Catalysis, vol. 2, VCH, New York, 1997, p. 707.
[39] J.M. López Nieto, R. Coenrads, A. Dejoz, M.I. Vázquez, Stud. Surf. Sci. Catal. 110 (1997) 767.
[40] T. Blasco, J.M. López Nieto, Appl. Catal. A 157 (1997) 117.
[41] B. Grzybowska-Swierkosz, Top. Catal. 21 (2002) 35.
[42] R.B. Watson, U.S. Ozkan, J. Catal. 191 (2000) 12.
[43] K. Chen, S. Xie, A.T. Bell, E. Iglesia, J. Catal. 195 (2000) 244.
[44] M. Takahashi, X. Tu, T. Hirose, M. Ishii, US patent 5,994,580 (1999).
[45] L. David, C. Craciun, M. Rusu, D. Rusu, O. Cozar, J. Chem. Soc., Dalton Trans. (2000) 4374.
[46] L. Luo, J.A. Labinger, M.E. Davis, J. Catal. 200 (2001) 222.
[47] M. Lin, T.B. Desai, F.W. Kaiser, P.D. Klugherz, Catal. Today 61 (2000) 223.
[48] T. Shishido, T. Konishi, I. Matsuura, Y. Wang, K. Takaki, K. Takehira, Catal. Today 71 (2001) 77.
[49] T. Seiyama, K. Nita, T. Mahehara, N. Yamazoe, Y. Takita, J. Catal. 49 (1977) 164.
[50] C. Martin, I. Martin, C. Mendizábal, V. Rives, Stud. Surf. Sci. Catal. 75 (1993) 1987.
[51] P. Forzatti, F. Trifiró, P.L. Villa, J. Catal. 52 (1978) 389.